Article

Not peer-reviewed version

Effects of Gamma Radiations on the I-V Electrical Parameters of a n-MOSFET

Dorsaf Aguir * and Mohsen Machhout

Posted Date: 14 May 2025

doi: 10.20944/preprints202505.1056.v1

Keywords: SOI n-MOSFET; Gamma radiations; I-V characteristics; Total Ionizing Dose; In-situ thermal annealing; Electron traps; static and dynamic parameters; Fitting

 doi:10.20944/preprints202505.1056.v1

Article

Effects of Gamma Radiations on the I-V Electrical Parameters of a n-MOSFET

Dorsaf Aguir * and Mohsen Machhout

Laboratory of Electronics and Microelectronics, University of Monastir (LEMM) Monastir, Tunisia

* Correspondence: author email: dorsafaguir7@gmail.com

Abstract: Hostile environments usually contain different types of ionizing radiations. In Si-based MOSFETs, radiation-induced defects can lead to drastical degradations in the relevant current-voltage characteristics. At the micro-scale, the capacitance reveals degeneration due to an accumulation of trapped holes within the oxide layer and at the oxide-channel interface. As a peculiar feature of this degeneration, several electrical parameters of the transistor are directly impacted by the variation in the gate-oxide capacitance. It has been found from experimental measurements that the threshold potential exhibits a negative shift as the absorbed gamma ray dose increases. As it is already suggested, the negative shift in the threshold potential results from a trapping of positive charges into the gate capacitance. In the present work, the trapping of holes is rather assumed to behave as a compensating donor center. Which leads to relate them into the acceptor doping concentration. In the paper, we have also investigated the electron transport under exposure to gamma radiations. For this purpose, we have developed a direct and a small-signal current models. From the I–V measurements, a set of fitting laws has been derived for both static and dynamic parameters as functions of the total ionizing dose. An explanation of the physical origin of the radiation-induced dysfunction is provided based on the behavior of the investigated n-MOSFET. Our findings offer valuable insights into the modeling and mitigation of power-related degradation, providing guidance for the design of energy-aware and radiation-hardened low-power electronic systems.

Keywords: SOI n-MOSFET; gamma radiations; I-V characteristics; total ionizing dose; in-situ thermal annealing; electron traps; static and dynamic parameters; fitting

1. Introduction and Related Works

During the last decades, a significant progress has been achieved in epitaxial growth and in the technological design as well for bipolar-junction and metal-oxide semiconductor FETs **[1–4]**. The challenge has been how to proceed in order to reducing the nuisible effects of imperfections. However, impurities and defects are always present in the host lattices, thus inducing localized extrinsic states in the active layers. Most process-induced traps behave as trapping centers, which lead to deposited positive charges. The origin of the active traps and especially their locations has been characterized using different techniques, but the proposals of explanations are still controversial. It is worth noticing that defects could be intrinsic or arising from an extrinsic origin. For MOSFET transistors operating in hostile environments, exposure to gamma radiations can cause many disturbances in their characteristics and functionality **[5–7].** Depending on TID doses, gamma radiations may induce a permanent failure in the transistor's characteristics. At the microscopic scale, these degradations have been explained as due mainly to an accumulation of trapped holes in the oxide layer and eventually at the oxide –channel heterointerface **[8]**. It is worth to mention that the trapped charge densities strongly depend on the device design architecture as well as on the technology process **[9]**. As a first alternative to mitigate the effects of trapped charges, irradiated transistors were subjected to an annealing at relatively high temperatures during prolonged periods

 doi:10.20944/preprints202505.1056.v1

of heating **[10,11]**. The major drawback of this annealing procedure is the high loss of thermal energy. In a recent work, an advanced recovery method has been conceived and realized using micro-integrated hotplates. This technique benefits from an excessive rapidity, a low power loss, and an in-situ electro-thermal annealing **[12,13]**. From a technological view point, it was revealed in addition that the immunity to transients of gamma radiations can be further improved by including buried-oxide (BOX) epilayers **[9]** in order to separate the thin Si active layer from the substrate. As has been found, this novel technique has led to a peculiar success in a partial or complete recovery of degradations for a large range of TIDs [12–14].

In the context of low power design, radiation-induced effects pose a significant challenge by increasing leakage currents, degrading subthreshold behavior, and shifting threshold voltages—all of which directly affect energy efficiency, system reliability, and power-aware operation. Understanding and modeling these effects is therefore crucial for designing robust, energy-efficient systems in hostile environments.

The aim of the present work is to investigate the effects of gamma radiations on the electron transport in a Si-based n-MOSFET with 1µm-lengh channel. Measurements of I-V at output have been performed before and after thermal annealing. From the relevant I-V at output, we have extracted the threshold voltage, the transconductance and the conductance as well. Theoretically, we have developed a direct-current (DC) and a small-signal (AC) models in order to analyze the electrical behavior of defected n-MOSFETs due to gamma radiations. As has been already reported in previous works, the effects of radiation-induced traps are included into an interfacial gate-oxide charge. Here, these effects are rather related to an effective concentration of the acceptors as regards to the free carriers in the conductive channel. The choice of the latter model is not far from being physically meaningful and $N_A^{eff.}$ can also be used as an useful technological parameter to describe the radiation hardening. From experimental data and using the (DC) and (AC) models, we have deduced the set of static and dynamic parameters for the n-MOSFET studied as a function of TID. The paper is organized as follows: After a brief introduction, we present in section II the direct-current and small-signal models. Results will be discussed in section III, and concluding remarks are summarized in section IV.

2. DC and Small-Signal Models for an n-MOSFET

2.1. The Direct-Current Model

In a field-effect transistor, the insertion of n+-doped contacts adjacent to the MOS capacitance makes that a current flow can occur between the two contacts only when the surfaces are inverted. As a main assumption, the oxide layer would contain a large number of fixed charges. For a sake of simplicity, the free carriers are assumed to have a constant mobility in the whole conductive channel, and the MOS heterostructure is in a flat band regime. Provided that the electron density has the form n=n(x,y), and by using the Ohm's law, the drain-to-source current will be given by:

$$\mathbf{I_{DS}} = -\mathbf{W}\mu_n \mathbf{Q_N(y)} \frac{\mathbf{dV(y)}}{\mathbf{dy}} \tag{1}$$

with

$$\mathbf{Q_N(y)} = -\mathbf{e}\int_0^{\Delta x_N} \mathbf{n(x,y)dx}$$

where μ_n is the electron mobility, $Q_N(y)$ and $V(y)$ are respectively the electron charge in the channel per unit area and the built-in potentiel at position y and Δx_N represents the channel penetration depth along the transversal x-axis. Note that I_{DS} is independent on the position y, which leads to the following analytical expression:

$$\mathbf{Q_N(y)} = -\frac{\boldsymbol{\varepsilon_0\varepsilon_{rox}}}{\mathbf{d}}[\mathbf{V_{GS}} - \mathbf{2\phi_{Fi}} - \mathbf{V(y)}] + \sqrt{\mathbf{2e\varepsilon_0\varepsilon_{rox}N_A}}[\mathbf{V(y)} + \mathbf{2\phi_{Fi}}] \tag{2}$$

 doi:10.20944/preprints202505.1056.v1

with

$$\boldsymbol{\phi_{Fi}} = \frac{\mathbf{K_{BT}}}{\mathbf{2e}} \mathbf{Ln} \frac{\mathbf{N_A}}{\mathbf{n_i s_i}} \quad (2)$$

where V_{DS} and V_{GS} are the drain-to-source and the gate-to-source bias potentials, L denotes the channel length ε_o ε_r and d represent respectively the dielectric permittivity and the thickness of the oxide layer, $\boldsymbol{\phi_{Fi}}$ is the Fermi potential , N_A is the doping concentration of acceptors and n_{isi} indicates the intrinsic concentration of the Si. As it clearly appears, the drain current is controlled by both V_{GS} and V_{DS}. Two peculiar parameters can be derived from the I_{DS}-V_{GS} and I_{DS}-V_{DS} :**(i)** The transconductance defined as $\mathbf{g_m} = (\frac{\partial \mathbf{I_{DS}}}{\partial \mathbf{V_{GS}}})_{\mathbf{V_{DS}}}$ **,(ii)** the conductance given by $\mathbf{g_d} = (\frac{\partial \mathbf{I_{DS}}}{\partial \mathbf{V_{DS}}})_{\mathbf{V_{GS}}}$

2.2. Drain Current in Linear and Saturation Regimes

2.2.1. Linear Regime

For this regime, it is convenient to adopt the following approximations:

(i)- $\mathbf{V_{DS}} \ll \mathbf{2\phi_{Fi}}$

(ii)- $\frac{\mathbf{V_{DS}}^2}{\mathbf{2}} \ll (\mathbf{V_{GS}} - \mathbf{2\phi_{Fi}})\mathbf{V_{DS}}$**.**

In such a case, the drain current expression reduces to:

$$\mathbf{I_{DS}}(\mathbf{V_{GS}}, \mathbf{V_{DS}}) = \frac{\mathbf{W\mu_n C_{ox}}}{\mathbf{L}} (\mathbf{V_{GS}} - \mathbf{V_{Th}})\, \mathbf{V_{DS}} \quad (3)$$

with $\mathbf{C_{ox}} = \frac{\boldsymbol{\varepsilon_0 \varepsilon_r}}{\mathbf{d}}$ is the oxide capacitance per unit area and $\mathbf{V_{Th}} = \mathbf{2\phi_{Fi}} + \frac{\mathbf{2}}{\mathbf{C_{ox}}} \sqrt{\boldsymbol{\varepsilon_0 \varepsilon_r e N_A \phi_{Fi}}}$ is the threshold voltage

As it is seen from **Eq.(3)**, the drain current shows a linear trend with increasing V_{DS} and V_{GS} respectively. For a fixed V_{DS} , however, the electron transport in the channel can occur only when V_{GS} exceeds the threshold potential V_{Th}. As for the transconductance and conductance in the linear regime, they are given by:

$$\mathbf{g_m}(\mathbf{V_{GS}}, \mathbf{V_{DS}}) = \frac{\mathbf{W\mu_n C_{ox}}}{\mathbf{L}} \mathbf{V_{DS}} \quad (4)$$

$$\mathbf{g_d} = \frac{\mathbf{W\mu_n C_{ox}}}{\mathbf{L}} (\mathbf{V_{GS}} - \mathbf{V_{Th}})$$

As can also be noticed from **Eq. (4)**, both $g_m$and g_d show a linear variation as a function of the V_{DS} and V_{GS} bias potentials.

2.2.2. Saturation Regime-Effect of the Channel Modulation

When V_{DS} exceeds the linear regime, the electron density $Q_N(y)$ decreases near the drain contact and therefore the current flow exhibits a sub-linear variation that tends towards the saturation regime. In terms of a biased voltage, this regime is reached if the channel pinch coincides with the drain. Which leads to write V_{DS} and I_{DS} under the forms*:*

$$\mathbf{V_{DS,SAT}}(\mathbf{V_{GS}}) = (\mathbf{V_{GS}} - \mathbf{V_{Th}}) \quad (5)$$

$$\mathbf{g_d} = \frac{\mathbf{W\mu_n C_{ox}}}{\mathbf{L}} (\mathbf{V_{GS}} - \mathbf{V_{Th}})$$

and $\mathbf{I_{DS,SAT}}(\mathbf{V_{GS}}) = \frac{\mathbf{W\mu C_{ox}}}{\mathbf{2L}} (\mathbf{V_{GS}} - \mathbf{V_{Th}})^2$

For a V_{DS} upper than $V_{DS,SAT}$,the excess voltage $\Delta V_{DS} = V_{DS}$-$V_{DS,SAT}$ is applied across a depleted region of width ΔL. The channel remains subjected to the $V_{DS,SAT}$ bias voltage while its length decreases as V_{DS} increases. This leads to an increasing of both the channel conductance and the drain current. Calculation by using the Poisson equation of I_{DS} as well as g_m and g_d gives rise to the set of relationships:

 doi:10.20944/preprints202505.1056.v1

$$I_{DS,SAT}(V_{GS},V_{DS}) = \frac{W\mu C_{ox}}{2L}\left[1+\frac{1}{L}\sqrt{\frac{2\varepsilon_0\varepsilon_r}{eN_A}(V_{DS}-V_{DS,SAT})}\quad\right](V_{GS}-V_{Th})^2$$

$$g_m = \frac{W\mu_n C_{ox}}{L}\left[1+\frac{1}{L}\sqrt{\frac{2\varepsilon_0\varepsilon_r}{eN_A}(V_{DS}-V_{DS,SAT})}\right]\ (V_{GS}-V_{Th}) \quad (6)$$

$$g_d = \frac{W\mu_n C_{ox}}{4L^2}\sqrt{\frac{2\varepsilon_0\varepsilon_r}{eN_A(V_{DS}-V_{DS,SAT})}}(V_{GS}-V_{Th})^2$$

In computing the drain current, ΔL is assumed to be less lower than L. As revealed from **Eq.6**, the I_{DS}-V_{DS} characteristics of an n-MOSFET exhibit an amount with increased V_{DS}, thus leading to a change of the parameters g_m and g_d. In closing this part of the DC model, let us recall that the n-MOSFET is assumed to be in the flat band regime. To overcome this insufficiency, it is required to take into account the output work due to the contact phenomenon. Correction could be made by defining the effective Fermi potential as: $e\phi_{Fi}^{eff.} = e\phi_{Fi} + e\phi_{MS}$.

2.3. Small-Signal Model

2.3.1. Resistive Operating

As it reveals from **Eq.3**, the direct-current characteristics in linear regime are approximated by a linear law relating I_{DS} to the drain-to-source bias voltage V_{DS}. In terms of an equivalent circuit scheme, the n-MOSFET is found to behave as a resistance whose value is controlled by V_{GS}.

$$R_{DS}(V_{GS}) = \frac{L}{w\mu_n C_{ox}(V_{GS}-V_{Th})} \quad (7)$$

In technological applications, the n-MOSFET in linear regime can be used as an on-off switch.

2.3.2. Operation as an Amplifier

For long channel transistors, the direct current characteristics in saturation regime can be approximately analyzed by using **Eq.5**. Two concluding remarks can be derived from this relation:

(i) The saturated drain-current does not depend on V_{DS} and shows a quadratic variation versus V_{GS}.
(ii) on the other hand, the n-MOSFET behaves as an ideal current source whose intensity is:

$$I_0 = \frac{W\mu_n C_{ox}}{2L}(V_{GS}-V_{Th})^2 \quad (8)$$

In reality, the channel of a n-MOSFET is modulated especially when V_{DS} exceeds $V_{DS,SAT}$. In such a case, the drain-current should be evaluated more rigorously from **Eq.6**. Opposite to the ideal current source, the inverse of g_d is finite an defines the output resistance as:

$$R_o(V_{GS},V_{DS}) = \frac{4L^2}{W\mu_n C_{ox}}\sqrt{\frac{eN_A(V_{DS}-V_{DS,SAT})}{2\varepsilon_0\varepsilon_r}}(V_{GS}-V_{Th})^2 \quad (9)$$

Association in parallel of both I_O and R_O gives rise to the output equivalent scheme at low frequencies of a small-signal n-MOSFET. Between the grille and source terminals, the circuit is opened. At high frequencies, however, capacitance effects should be accounted for. An improved equivalent circuit of a n-MOSFET amplifier is reported in **Figure 1**.

Preprints.org (www.preprints.org) | NOT PEER-REVIEWED | Posted: 14 May 2025 doi:10.20944/preprints202505.1056.v1

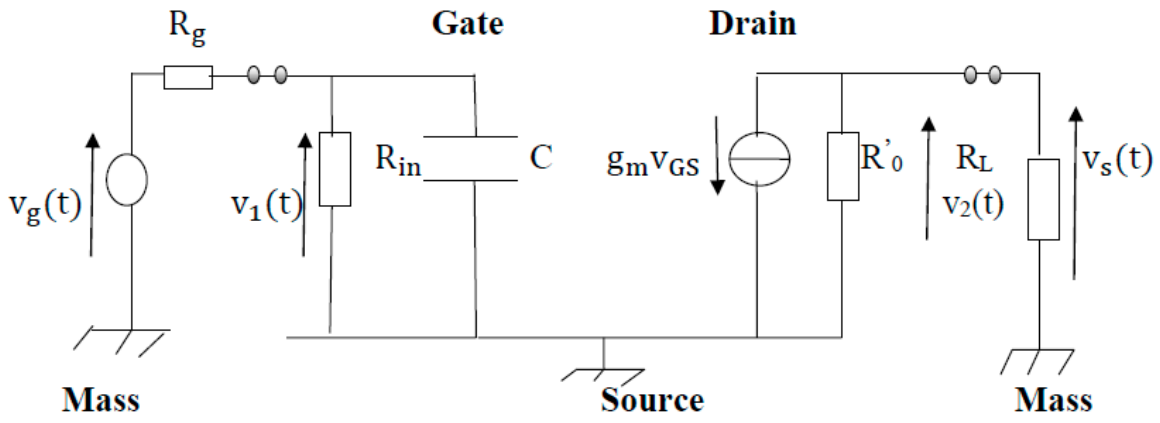

Figure 1. Equivalent circuit at high frequencies of an n-MOSFET amplifier with: $\mathbf{R_{in} = R_{G1}//R_{G2}}$. $\mathbf{C = \frac{1}{2}(2 + g_m R'_0)WLC_{ox}}$ and $\mathbf{R'_0 = R_0//R_D}$.

The term $g_m v_{GS}$ represents the intensity of input-output controlled source. Both of elements v_g and R_g correspond to the voltage source applied at input of the MOSFET transistor. Wearers R_{G1}, R_{G2} and R_D are the biased resistances connected to the gate and drain contacts. As for R_L and C they denote the load resistance and the total capacitance at input. To predict the frequencial behavior of a small-signal transistor amplifier, it is required to define its imput and output impedances as well as its current and voltage gains. Such operating characteristics can be determined using the hybrid parameters. For the n-MOSFET investigated, the latter parameters are given by the set of equations:

$$\mathbf{h_{11} = \frac{R_{in}}{1 + jR_{in}\, c\omega}}$$

$$\mathbf{h_{12} = 0}$$

$$\mathbf{h_{21} = \frac{-g_m R_{in}}{R_g + R_{in}\, c\omega}} \tag{10}$$

$$\mathbf{h_{22} = \frac{1}{R'_0}}$$

As a striking feature of the hybrid parameters, the input and output parts of the equivalent circuit seem to be isolated but their coupling is accounted for by means of the controlled source $h_{21}v_1$. This makes the n-MOSFET amplifier easily to be modeled into a device network. For a load charge R_L connected at output, calculation of the dynamic parameters leads the h_{ij}-dependent expressions:

$$\mathbf{Z_{in} = h_{11}}$$

$$\mathbf{A_v(\omega) = \frac{h_{21}}{h_{11}(h_{21} + \frac{1}{R_L})}}$$

$$\mathbf{A_i = \frac{h_{21}}{1 + h_{22}R_L}} \tag{11}$$

$$\mathbf{Z_{out} = \frac{1}{h_{22}}}$$

Under the circumstance $h_{22}R_L \ll 1$, it is beneficial to use approximate formulas for the dynamical parameters:

$$\mathbf{Z_{in} = h_{11}}\ ;\mathbf{A_v = -\frac{h_{21}R_L}{h_{11}}}\ ;\ \mathbf{A_i = h_{21}};\ \ \mathbf{Z_{out} = \frac{1}{h_{22}}} \tag{12}$$

 doi:10.20944/preprints202505.1056.v1

As it would be expected from the simplifying assumption, the feedback effect ot output into input can be disregarded in an operating transistor. Which has led to omit the controlled source $h_{12}v_2$ in the equivalent hybrid parameter circuit. On the other hand, values of hybrid parameters and their related dynamical characteristics strongly depend on the transistor connection. From the transfer function $H(j\omega) = \frac{v_2}{v_1}$, we have also deduced the cutoff frequency:

$$\omega_c = \frac{1}{R_{in}C} \tag{13}$$

3. Static and Dynamic Characteristics of an Irradiated n-MOSFET

3.1. Static Parameters

The n-MOSFET under investigation has been fabricated using 1µm partially depleted SOI technology. The transistor device is implemented in a 600 µm diameter circular membrane. Both are located near a micro-heater used for in-situ thermal annealing. Two auxiliary PIN diodes are placed on the membrane to monitor the temperature during operation. A detailed description of the fabrication process and the annealing procedure are available in Ref. **[12]**. Concerning the electrical characteristics, drain current has been measured versus the gate-to-source voltage V_{GS} in both linear and saturation regimes for V_{DS}fixed at 50 mV and 3 V, respectively. Measurements were performed before and after gamma radiations. **Figure 2** shows I_{DS} as measured versus V_{GS} in the range 0-3V pre- and post-radiation. The drain source V_{DS} potential is maintained at 50 mV.

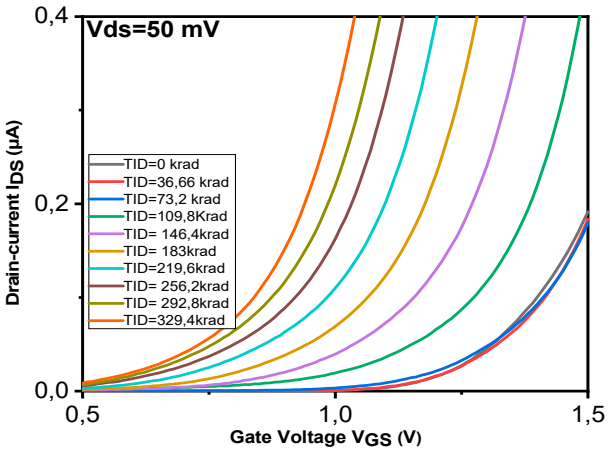

Figure 2. Drain-current versus the gate-voltage in the linear regime for different TIDs.

As can be seen, the I-V characteristics show a negative shift as the TID increases in the 36.66 Krad- 329.4 Krad range. From a linear extrapolation, we have extracted the threshold-potential V_{Th}. Results are reported in **Figure 3**.

 doi:10.20944/preprints202505.1056.v1

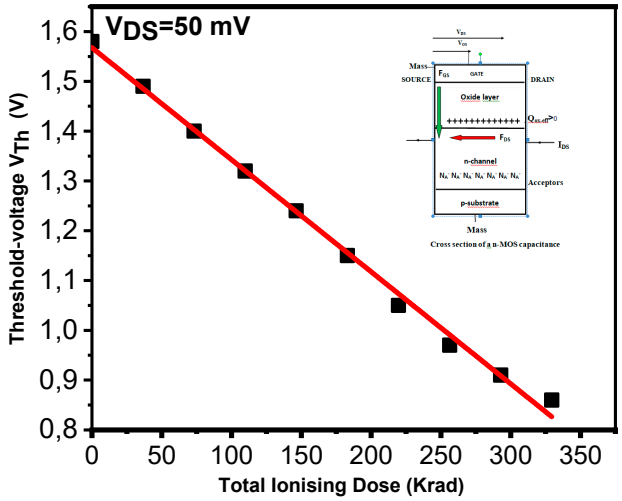

Figure 3. The threshold-voltage as a function of the Total Ionizing Dose in the linear regime.

It clearly appears that the threshold-potential V_{Th} shows a decreasing tendency as TID increases. Using a linear fit, the threshold potential V_{Th}(TID) reads in the linear-regime as:

$$\mathbf{Vth(TID)} = \mathbf{1.57 - 225\ 10^{-5} \times TID} \qquad \mathbf{inVOLT} \tag{14}$$

As reported in Ref.**[12]**, the threshold voltage shift ΔV_{th} is expected to result from a trapping of positive charges inside the oxide layer and at oxide n-channel. Let Q_{ox-eFF} be the total density of oxide-and interface-trapped holes per unit area, ΔV_{th} is related to $Q_{ox\text{-}eff}$ using the model **[12]**:

$$\mathbf{Q_{ox} = -C_{ox}\Delta V_{th}} \tag{15}$$

with $\mathbf{\Delta V_{th} = V_{th}(TID) - V_{th}(TID = 0)}$

From V_{th}=V_{th}(TID), we have deduced the interfacial gate-oxide density $Q_{ox\text{-}eFF}$ versus TID. Obtained results are shown in **Figure 4**.

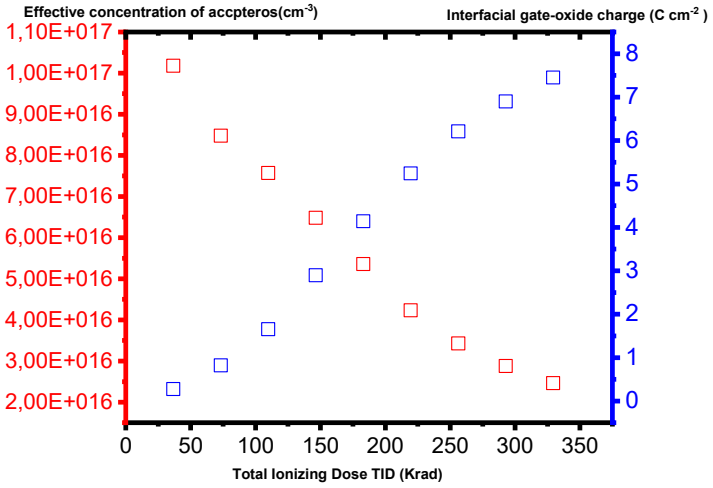

Figure 4. Effective concentration of acceptors and interface gate-oxide density as a function of Total Ionizing Dose.

As it is found, $Q_{ox\text{-}eff}$ shows an amount with increased gamma radiation dose. In terms of an analytical fitting, its expression is as follows:

 doi:10.20944/preprints202505.1056.v1

$$\mathbf{Q_{ox-eFF}(TID) = \ 0.06 - 0.0019 \ \times TID + 2\ 10^{-4} \times TID^2 - 3,85\ 10^{-7} \times TID^3} \qquad (16)$$

As an illustrative picture, we report in the inset of **Figure 3** the cross section of the MOS capacitance for a n-MOSFET under bias potentials V_{GS} and V_{DS}. The inset clearly shows the deposited interfacial holes under the effect of F_{GS} electric field. On the other hand, radiation hardening technologies reveal that thin gate oxide designs have a large capacitance which leads to a reduced threshold voltage shift. In terms of quantum tunneling, thin gate-oxide transistors favour the recombination of trapped holes with electrons initially located in the channel **[15,16]**. This can efficiently help MOSFET devices with thin gate-oxide thicknesses to become more hardened against hostile radiating environments. From the inset of **Figure 3**, it is seen that the n-channel is located between ionized acceptors in Si-substrate and trapped holes. Physically, this implies that free electrons in the conductive channel are jointly subjected to a double electrostatic interaction. In terms of equilibrium charge balance, acceptors can be considered as partially compensated by equivalent donor centers. This leads to define an effective density of the doped acceptors as $N_A^{eff.} = \alpha N_A$ where α represents the centesimal percent of compensation. According to this relation, the threshold voltage shift can be expressed as a function of $N_A^{eff.}$ using the new model:

$$\mathbf{\Delta V_{Th}(TID) = K[-1 + \sqrt{\frac{N_A^{eFF.}}{N_A}})]} \qquad (17)$$

with $\mathbf{K = \frac{2}{C_{ox}}\sqrt{\varepsilon_0 \varepsilon_r e N_A \phi_{Fi}}}$.

In establishing this relation, we have assumed that K does not vary significantly with TID. For the parameters N_A, n_{isi} and C_{ox}, we have taken the corresponding values 1.1710^{17}cm^{-3}, $1,510^{10}$ cm^{-3} and 1.3810^{-3} Fm^{-2} respectively. From the measurements of V_{th} versus TID in the linear regime, we have deduced $N_A^{eff.}$and results are summarized in **Figure 4**. As clearly shown, $N_A^{eff.}$ exhibits a decreasing trend as the gamma radiation dose increases. Analytically, the effective doping concentration of acceptors is fitted by a quadratic law according to:

$$\mathbf{N_A^{eFF.}(TID) = 1.17 - 4.34\ 10^{-2} \times TID + 4.56\ 10^{-6} \times TID^2} \quad \text{in} \quad \mathbf{10^{-17}}\ \text{cm}^{-3} \qquad (18)$$

So that, the choice of N_A^{eff} seems to being physically meaningful as $Q_{ox\text{-}eff}$ to analyze the electron transport in an irradiated n-MOSFET. From I_{DS}=$I_{DS}(V_{GS})$ measurements in the linear regime, we have also extracted the transconductance. The relevant results are depicted in **Figure 5**.

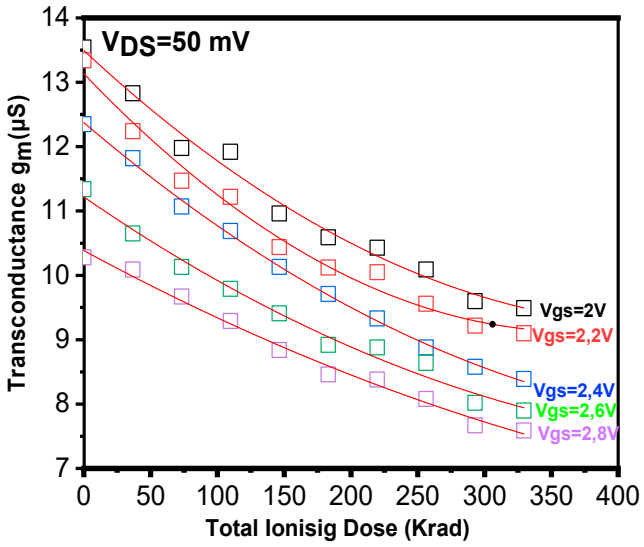

Figure 5. The transconductance as measured versus Total Ionizing Dose in the linear regime.

 doi:10.20944/preprints202505.1056.v1

Two peculiar features were revealed: **(i)** For a fixed V_{GS} the transconductance decreases with increased TID, **(ii)** Under a gamma radiation dose, the transconductance decreases as the gate-to-source voltage increases. On the other hand, the transconductance can be fitted by the TID-dependent expression:

$$\mathbf{g_{mLR}(TID) = a_0 + a_1 \times TID + a_2 \times TID^2}$$

$$\begin{aligned} \mathbf{a_0(V_{GS}) &= 21.92 - 4.085 \times V_{GS}} \\ \mathbf{a_1(V_{GS}) &= 0.0412 - 0.104 \times V_{GS}} \\ \mathbf{a_2(V_{GS}) &= 5.88\,10^{-5} + 1.79\,10^{-5} \times V_{GS}} \end{aligned} \quad (19)$$

In the saturation regime, however, measurements of the drain current have been carried out as follows. **Figure 6** depicts the relevant I_{DS} versus TID for different applied V_{GS} ranging from 1V to 3V.

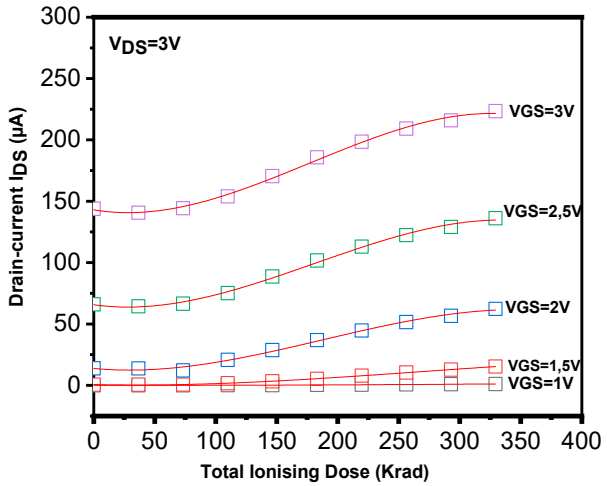

Figure 6. The drain-current versus Total ionizing Dose in the saturation regime.

The drain is subjected to a fixed bias voltage V_{DS}=3V. The plots reveal that: **(i)** for a V_{GS} lower than 1.5V which corresponds to the threshold potential, the drain current does not show a significant change as the TID varies, **(ii)** Beyond this value, I-V at output exhibits, in contrary, an increasing tendency as TID increases. As it is also noted, the increasing of I_{DS} is more noticeable with increased V_{GS}. Similarly to I_{DS} in the linear regime, saturated I-V characteristics are found to be fitted as a function of TID by a polynomial law with V_{GS} -dependent coefficients.

$$\mathbf{I_{DS,sat}(TID) = a_0 + a_1 \times TID + a_2 \times TID^2 + a_3 \times TID^3}$$

$$\begin{aligned} \mathbf{a_0(V_{GS}) &= 87.37 - 138.59 \times V_{GS} + 52.27 \times V_{GS}^2} \\ \mathbf{a_1(V_{GS}) = a_1(\mu A \times Krad^{-1}) &= 0.114 - 0.120 \times V_{GS} + 8.2510^{-3} \times V_{GS}^2} \\ \mathbf{a_2(V_{GS}) &= 2.88\,10^{-3} + 2.29\,10^{-3} \times V_{GS} - 1.54\,10^{-4} \times V_{GS}^2} \\ \mathbf{a_3(V_{GS}) &= 3.48\,10^{-6} - 3.4610^{-6} \times V_{GS} + 7.28\,10^{-8} \times V_{GS}^2} \end{aligned} \quad (20)$$

An attempt to explain the latter results will be subsequently proposed. The first feature is predictable since the conductive channel is not yet formed below the threshold potential. While the increase in I_{DS} as observed for V_{GS} greater than V_{th} is due presumably to the flow of an excedent of free electrons originating from hole-electron pairs created at the vicinity of the channel in Si-substrate, In n-MOSFET transistors exposed to high TIDs, it is worth noting that this dysfunction can lead to a derivation of the operating point. From I-V measurements performed in the saturation regime, we have deduced as well the transconductance versus TID and V_{GS}, see **Figure 7.**

Preprints.org (www.preprints.org) | NOT PEER-REVIEWED | Posted: 14 May 2025 doi:10.20944/preprints202505.1056.v1

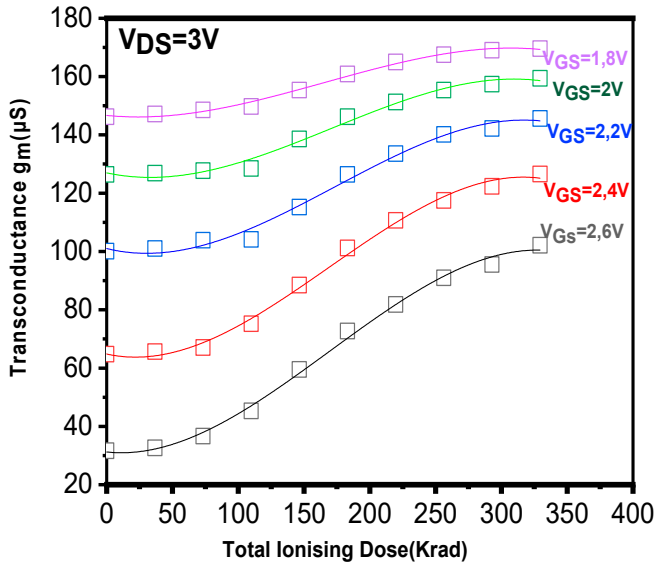

Figure 7. The transconductance as measured versus TID in the saturation regime.

As a main observation, the transconductance shows an increasing trend with increased TID. From a polynomial fitting, it was found that the transconductance can be written under the form:

$$\mathbf{g_{mSR}(TID) = a_0(V_{GS}) + a_1(V_{GS}) \times TID + a_2(V_{GS}) \times TID^2 + a_3(V_{GS}) \times TID^3}$$

$$\mathbf{a_0(V_{GS}) = -288.2 + 146.52 \times V_{GS}} \quad (21)$$

$$\mathbf{a_1(V_{GS}) = 0.149 - 0.117 \times V_{GS}}$$

$$\mathbf{a_2(V_{GS}) = 4.32\ 10^{-3} - 1.13\ 10^{-5} \times V_{GS}}$$

$$\mathbf{a_3(V_{GS}) = 7.98\ 10^{-6} + 1.99\ 10^{-6} \times V_{GS}}$$

The latter static parameter to being deduced is the conductance. As an experimental support, the drain current I_{DS} has been measured versus V_{DS} only for TID=0 Krad and TID=348 Krad. The gate voltage is fixed at V_{GS} =3V. From the relevant I-V characteristics, we have determined the conductance versus V_{DS}. Results are shown in **Figure 8**.

 doi:10.20944/preprints202505.1056.v1

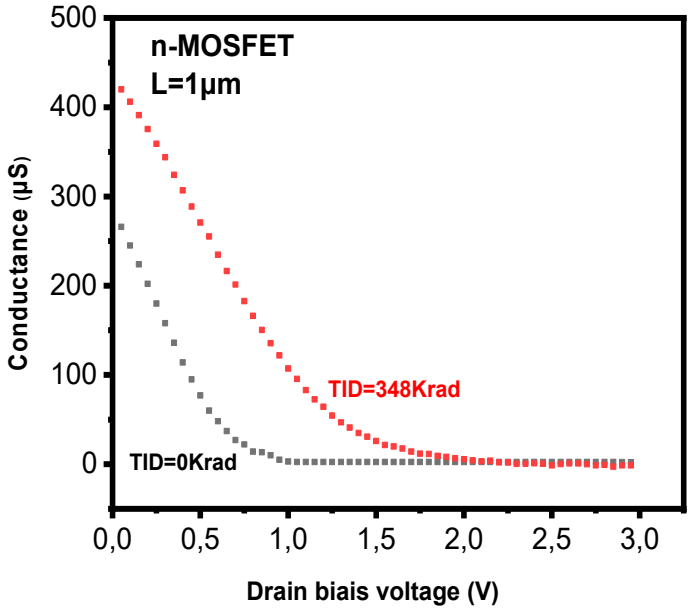

Figure 8. The VDS-dependent conductance as obtained for TID=0 Krad and TID=348 Krad.

It is thus found that the conductance shows a large amount with respect to that at TID=0 Krad for V_{GS} inferior to 2 V, which corresponds to $V_{DS,SAT}$ .In the saturation regime, however, the conductance does not exhibit a significant change under the impact of gamma radiations. Note that, in the absence of experimental data for intermediate TIDs, it has not been possible to achieve a direct fitting. But the TID-dependence of this parameter can be derived from the transconductance by using the relationships

$$\mathbf{g_{DLR}(TID) = g_{mLR}(TID)} = \frac{\mathbf{V_{GS}-V_{th}}}{\mathbf{V_{DS}}} \quad \text{for} \quad V_{DS}<V_{DS,SAT} \tag{22}$$

$$\mathbf{g_{DSR}(TID)} = \mathbf{g_{mSR}(TID)}\ \frac{\mathbf{g_{mSR}^2}}{\mathbf{4W\mu_n C_{ox}}}\sqrt{\frac{\mathbf{2\varepsilon_0\varepsilon_{rsc}}}{\mathbf{eN_A V_{DS}-V_{GS}+V_{th}}}} \quad \text{for} \quad V_{DS} >V_{DS,SAT}$$

The hreshold-potential $\mathbf{V_{Th}}$ and the transconductance in both regimes $\mathbf{g_{mLR}}$ and $\mathbf{g_{mSR}}$ have been calculated as a function of **TID** above.

3.2. Hybrid and Dynamic Parameters

A deal of interest has also been paid to the dynamic characteristics under the impact of gamma radiations. In section **II**, the hybrid parameters of the non- irradiated n MOSFET are defined by **Eq. (10)**. As it is seen, they are related to the transconductance g_m, the total capacitance C and the resistance R_O at output. Note that these static parameters are affected by the TID. From **Eq. (10),** we can deduce the modulas of the hybrid parameters as a function of TID.

$$\mathbf{h_{11}(TID)} = \frac{\mathbf{R_{in}}}{\sqrt{\mathbf{1+R_{in}^2 C^2(TID)\omega^2}}} \tag{24}$$

$$\mathbf{h_{12} = 0}$$

$$\mathbf{h_{21}(TID) = g_m(TID) * h_{11}(TID)}$$

$$\mathbf{h_{22}(TID)}=\frac{\mathbf{1}}{\mathbf{R_D}} * \frac{\mathbf{1}}{\mathbf{R_O(TID)}}$$

The TID-dependence of the dynamic parameters can be established as well using the set of relations:

$$\mathbf{Z_{in}(TID) = h_{11}(TID)} \tag{25}$$

 doi:10.20944/preprints202505.1056.v1

$$\mathbf{A}_{\mathbf{v}}(\mathbf{TID}) = \frac{\mathbf{h_{21}(TID)R_L}}{\mathbf{h_{11}(TID)}}$$

$$\mathbf{A_i(TID)} = \mathbf{h_{21}(TID)}$$

$$\mathbf{Z_{out}(TID)} = \frac{\mathbf{1}}{\mathbf{h_{22}(TID)}}$$

$$\boldsymbol{\omega}_{\mathbf{c}}\mathbf{(TID)} = \frac{\mathbf{1}}{\mathbf{C(TID)R'_{in}}}$$

For the bias-resistances in the static regime, we have taken R_{G1}=R_{G2}=10MΩ and R_D=10KΩ. Wherares the operating frequency is fixed at N=100 GHz, which corresponds to ω=6.28$10^{11}$ rds^{-1}. The gate-to-source voltage V_{GS} is treated as an adjustable variable. Using **Eqs (24)** and **(25)**, we have computed the hybrid parameters and their related dynamic characteristics for the n-MOSFET investigated versus TID and V_{GS}. **Figure 9** depicts the plots as obtained in the TID range 36.66 Krad - 329.6 Krad and for V_{GS} fixed at 2V and 3V respectively which correspond to the amplifier operating regime. As has been found: **(i)** For V_{GS} =2V, both the hybrid and dynamic parameters show a significant change under the effect of gamma radiations particularly at high gamma-ray doses, **(ii)** They, however, seem to be less impacted under the same TIDs at V_{GS} =3V.

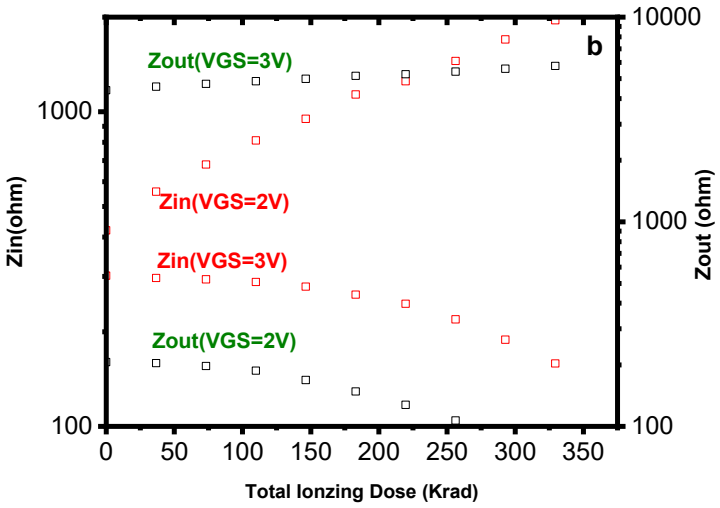

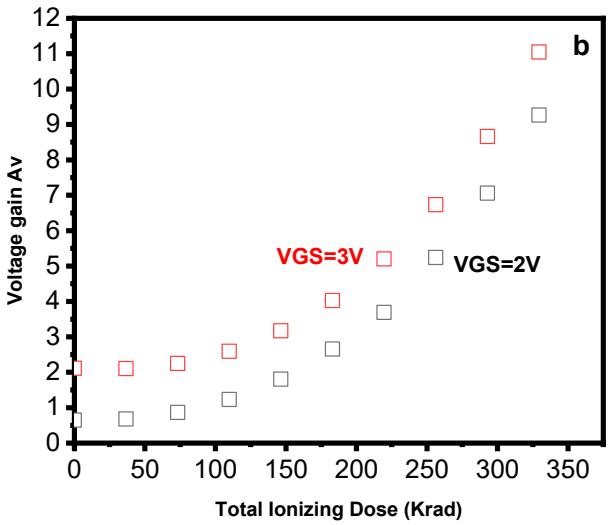

 doi:10.20944/preprints202505.1056.v1

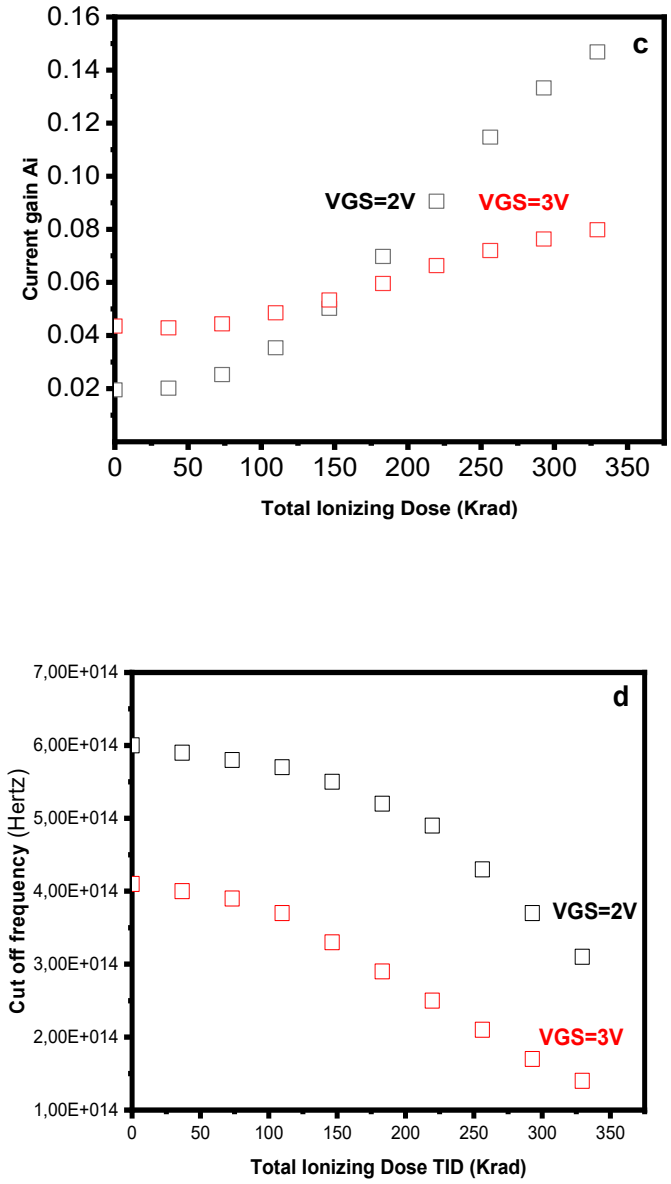

Figure 9. imput/output Impedances **(a)**; Current/Voltage Gains **(b-c)** and Cutoff Frequency **(d)** versus TID for V_{GS}=2V and 3V respectively.

4. Summary and Conclusions

The present work is aimed to investigate the effects of gamma-absorbed radiations on the electron transport in an n-MOSFET grown on SOI membrane. The electrical behavior of the transistor is characterized using direct-current measurements. From the relevant results, it has been shown that exposure to a relatively high gamma-ray dose can lead to a drastic degradation of the MOSFET characteristics at output. As a proposal of explanation, these degenerations are assigned to an accumulation of trapped holes in the gate-oxide and at the oxide-channel interface. Here, the trapping of charges is modeled in terms of a compensating donor center. Which has led to defining the effective concentration of acceptors by including the trapping effects. As a direct impact of gamma radiations, the threshold potential is shifted and both the transconductance and conductance are dysfuntioned. Theoretically, we have developed a direct-current model to simulate the static parameters as a function of the total ionizing dose. As an experimental support, a series of I-V measurements were performed at room temperature before and after gamma irradiation. From a polynomial fitting, it has

 doi:10.20944/preprints202505.1056.v1

been possible to establish a set of TID-dependent empirical laws for these parameters. A deal of interest has also been paid to the impacted dynamic characteristics. Using a small-signal model, we have deduced the hybrid parameters and their related input and output impedances as well as voltage and current gains. The last step of the simulation has been dedicated to computing the TID-dependent cutoff frequency. The n-MOSFET under investigation is assumed to operating as an amplifier. Two main conclusions can be drawn: (i) For a fixed VGS of 2 V, all dynamic parameters are strongly affected by gamma radiation, (ii) the change in electrical behavior becomes less pronounced for higher VGS values. In contrast, the cutoff frequency degrades steadily for both VGS conditions. These results demonstrate that gamma-induced degradation mechanisms directly impact performance and reliability in low-power applications. Increased leakage and reduced gain at typical biasing conditions highlight the vulnerability of energy-constrained systems in radiation-prone environments. Consequently, the modeling and empirical laws derived in this work are expected to support the development of radiation-hardened, energy-aware design strategies for low-power MOSFET-based electronics.

References

1. H.J. Barnaby, R. D. SchrimpF, A. L. Sternberg, V. Berthe, C. R. Cirba and R.L Sci. 48 (2001) Proton radiation response mechanisms in bipolar analog circuits. Please, IEEE trans. Nucl. pp 2074.
2. M. Menichelli, B. Alpata , R. Batliston , M. Bizzarri, S. Blasko, L. Massoa , E.M Fioria, A. Papia and G.Scalieri, Radiation damage of electronic components to be used in a space experiment, Nuclear Physics B 113 (2002) pp 310.
3. N. Pushppa , K.C. Praveen , A. P. Gnana Prakash , Y. P. Prabhakara Rao , Ambuj Tripati and D. Revanna siddaich , A comparison of 48 MeV Li^{3+} ion, 100 MeV F^{8+} ion and Co-60 gamma irradiation effect on N-channel MOSFET Nucl. Instr. Meth. Res. A 613 (2010) pp 280.
4. A.Anjum , N.H. Vinayakprasanna , T. M.Pradeep, N. Pushpa, J.B.M. Krishna and A. P. Gnana Prakash, A comparison of 4 MeV Proton and Co-60 gamma irradiation induced degradation in the electrical characteristics of N-channel MOSFETs, Nucl. Instr. Meth. Res. B 379 (2016) pp 265.
5. R. Freeman and A. Holmes-Siedle, A simple model for predicting radiation effects in MOS devices,IEEE Trans. Nucl. Sci. 25 (1978) pp 1216.
6. J. M. Benedelto, H. E. Boesch and F. B. Mclean, Dose and energy dependence of interface trap formation in cobalt-60 and X-ray environments, IEEE Trans. Nucl. Sci. 35 (1988) pp 1260.
7. M. Soubra, J. Cygler and G. Maskay, Med, Evaluation of a dual bais dual metal oxide-silicon semiconductor field effect transistor detector as radiation dosimeter, Phys. 21 (1994) pp 567.
8. T.R. Oldham and F. B. Mclean, Total ionizing dose effects in MOS oxides and devices, IEEE Trans. Nucl. Sci-50 (2003) pp 483.
9. J. Alvarado, V. Kilchtska, E. Boufouss, Soto- Guz and D. Flandre, A compact model for single event effects in PD SOI sub-micron MOSFETs, IEEE Trans. Nucl. Sci. 59 (2012) pp 943.
10. C. Gwyn, Model of radiation-induced charges trapping and annealing in the oxide layer of MOS devices, Journal of Applied Physics 40 (1969) pp 4886.
11. M. M. Pejovic and A. B. Jaksic, Contribution of fixed oxide traps to sensitivity of pMOS dosimeters during gamma ray irradiation and annealing at room and elevated temperature, Sensors and Actuators A: Physical 174 (2012) pp 85.
12. S. Amor, N. André, V. Kilchytska, F. Tounsi, B. Mezghani, P. Gérard, Z. Ali, F. Udrea, D. Flandre and L. A. Francis, In situ-Thermal Annealing of On-Membrane SOI Semiconducteur-Based Devices After High Gamma Dose irradiation, Nanotechnology 28 (2017) pp 184.
13. S. Amor, V. Kilchytska, D. Flanfre and P. Galy, The recovery by in situ-annealing in fully-delepted MOSFET with active silicide resistor, IEEE Electron Device Letters 42 (2021) pp 1085.
14. A. F. Laurent, S. Amor, A. Nicolas, K. Valeria, G. Pierre, A. Zeeshan, U. Florin and F. Denis, A Lower – Power and In Situ Annealing Technique for the recovery of Active Devices After Proton Irradiation, EPJ Web of Conferences 170 (2018) pp 01006.

 doi:10.20944/preprints202505.1056.v1

15. N.S.Saks, M.G.Ancona and J.A.Modolo, Generation of interface states by ionizing radiation in very thin MOS oxides, IEEETrans. Nucl. Sci. 33 (1986) pp1185.
16. V.Gromov , A.J.Annema, R.Kluit ,J.l. Visschers and P.Timmer , Aradiation hard bandgap referece circuit in a standard 0.13μm CMOS Technology ,IEEE Trans. Nucl. Sci. 54(2007) pp2727.